RSC Advances

ROYAL SOCIETY OF CHEMISTRY

www.rsc.org/advances

Denitrification Utilizing a Vaporized Enhanced-Fenton Reagent: Kinetics and Feasibility

Yi Zhao *, Runlong Hao

（School of Environmental Science and Engineering, North China Electric Power University, Baoding 071003）

Abstract This paper proposed a novel integrative process for NO removal, in which, NO was initially oxidized by a vaporized enhanced-Fenton reagent (EF) composed of hydrogen peroxide, ferrous and peroxyacetic acid (PAA) then absorbed by $Ca(OH)_2$. The effects of EF constitution, the reaction temperature, the pH of EF solution and the SO_2 concentration on NO removal were investigated systematically, and the experimental results indicated that both of $FeSO_4$ and PAA can significantly promote the oxidation rate of NO; the decreasing pH and the increasing temperature played a key role in enhancing NO removal. The NO depletion exhibited a pseudo-first-order kinetics pattern in 1-2 half-lives based on the macrokinetics of NO oxidation. And the rate constants determined in the temperature range of 60 to 120 ^{o}C were well fitted to the Arrhenius equation, yielding the apparent activation energy of 14.1 kJ/mol. The mechanism of NO oxidation was also speculated.

Keywords Denitrification; Kinetics; Enhanced-Fenton reagent; Feasibility analysis; Apparent activation energy

1 Introduction

The SO_2 and NO of coal combustion gases emitted from the thermal power stations have brought great harm to the human health and the ecosystem; therefore, both of them have been received considerable concern in recent years. As the largest

coal-fired country in the world, Chinese government has tried the best effort to control the air pollution, and a large number of Wet Flue Gas Desulfurization systems (WFGD) and Selective Catalytic Reduction systems (SCR) have been installed for flue gas treatment of coal-fired power plants. Whereas, the SCR-WFGD lay-out has the large and complex systems, and the high capital and operating costs, so the simultaneous removal technology that has the characters of simplified equipment, the smaller occupying areas and the lower operating cost has a good development and application prospect, in which, several advanced flue gas treatment technologies, such as the electrochemistry [1-2], the gas solid phase adsorption [3-4], the gas solid phase catalysis [5-6], the liquid phase absorption [7-8] and the liquid phase oxidation [9-17] were attempted for simultaneous removal of SO_2 and NO. However, because of the high costs or technical problems, these simultaneous removal technologies can not still completely replace the combination of WFGD and SCR technologies. Therefore, to develop new flue gas treatment technologies has become one of the major development trends in the coal-fired flue gas control field.

Compared with other developing methods, the oxidation method seems to be one of the promising ways for simultaneous removal of SO_2 and NO, the core of which is to rapidly oxidize the insoluble NO to NO_2, and then absorbed by the followed flue gas Circulation Fluid Bed (CFB) or WFGDs. The potential reagents can be used in the oxidation process include O_3, $KMnO_4$, $NaClO_2$, NaClO, $K_2S_2O_8$, $KFeO_4$ and H_2O_2, etc [7-10, 18-20]. However, some of the classical oxidants either have the lower economical efficiencies or may release several hazardous byproducts that can

adversely affect the environment. For example, sodium chlorite is considered as one of the most effective reagents, but it is estimated that about 1.38 pounds of $NaClO_2$ is needed to remove 1 pound of NO_x; therefore, its cost is of prohibitive. In addition, high removal efficiency of NO can also be obtained by using permanganate; however, its cost is too high to be applied in the industry. What's worse, a large number of heavy metals, manganese and chlorine species that can cause secondary pollution will remain in the removal products. Ozone is an environmentally benign and effective gas oxidant, but the energy consumption of its generation is too excessive. Therefore, the development of innovative absorbent for NO removal is urgency, and the research emphasis should focus on the following three aspects: the relative lower cost, the high removal efficiency and the less secondary environmental impact.

Given the above requirements, H_2O_2 is likely to be the most suitable basic oxidant due to the superiorities of environmental friendly and lower price. However, its weak oxidizability makes it difficult to effectively and completely oxidize NO. For this, in the paper, we selected peroxyacetic acetic (PAA) and ferrous as the additives to enhance the oxidizing ability of H_2O_2 and then prepared a H_2O_2-based complex oxidant (CO). In addition to that, a novel flue gas cleaning process was proposed, in which, NO was initially oxidized to NO_2 by vaporized CO and then absorbed by $Ca(OH)_2$. To our knowledge, there were no reports in the field of NO removal on the usage of the vaporized CO as well as the novel approach.

The main objective of our research is to evaluate the macrokinetics and technical feasibility of the novel process on removing NO, so the bench scale kinetics tests

were conducted to determine reaction order and apparent activation energy with respect to NO; factors affecting the treatment, including the CO constitution, the pH of CO solution, the reaction temperature and the SO_2 concentration, were assessed.

2 Materials and Experiments

2.1. Reagents and Preparation of CO Solution

The reagents used were analytical grade (Kermel Company, Tianjin). 30% (w/w) of H_2O_2, 16% (w/w) of PAA and 99% (w/w) of $FeSO_4 \cdot 7H_2O$ were used to prepare CO solution, in which the fresh solutions of $FeSO_4$, PAA and H_2O_2 were added in a beaker in turn by using pipettes (10-1000 μl and 1-5 ml) and then shaken mildly. And its pH was adjusted by 1 mol/L of H_2SO_4 and 1 mol/L of NaOH. In addition, $Ca(OH)_2$ was employed as the absorbent for absorbing the reaction products of NO, and anhydrous $CaCl_2$ was used the dryer to avoid the damage of flue gas analyzer.

2.2. Experimental apparatus and procedures

The bench scale experiments were carried out through a self-designed experimental system, which mainly consisted of the simulated flue gas generation, the vaporization of CO solution, the integration of preoxidation and absorption and the tail gas detection, as shown in Fig. 1. The simulated flue gas was generated from N_2, SO_2, NO, O_2 and CO_2 provided in the compressed cylinders (1-5) (North special gas company, Baoding). A peristaltic pump (12) (BT100-1F，Longerpump，Baoding) was employed to pump CO solution (11) into the vaporization device of CO solution (9) that was heated by a thermal control electric heater (10) (ZDHW, Zhongxingweiye company, Beijing). The reactor was an U-type quartz tube (14) with a length of 30 cm

and an inner diameter of 2.5 cm, heated by a thermostat oil bath (16) (DC-RB, Duchuang technology company, Beijing). The temperatures of vaporization device (9) and reactor were detected by thermal couples. The inlet and outlet flue gas were detected by a flue gas analyzer (18) (ECOM-J2KN, RBR Company, Germany), which can detect various gases such as O_2 in a range of 0-21% (±0.01%), CO in a range of 0-10000 ppm (±10 ppm), NO in a range of 0-5000 ppm (±1 ppm), NO_2 in a range of 0-1000 ppm (±1 ppm) and SO_2 in a range of 0-5000 ppm (±1 ppm), in a working temperature range of 25-85 ^oC. The pH of CO solution was detected by a pH meter (PHS-3C, Youke company, Shanghai).

During the experiments, NO and N_2 were metered through mass flow controller (6) and mixed in a buffer bottle (7), in which NO and other coexistence gases were diluted by N_2 to the desired concentrations, from which the simulated flue gas was formed. Then the CO solution (11) was pumped by peristaltic pump (12) into the vaporization device (9), where it was vaporized immediately. At the same time, the vaporized CO carried by the simulated flue gas oxidized NO in the reactor (14). Finally, the unreacted oxidants, the iron precipitates and NO_x were absorbed by $Ca(OH)_2$ supported on the glass wool. The method for controlling NO oxidation time was designed as followed. Based on the volumes of the reactor and the vaporization device and the inlet flue gas flow, the time (Δt) that NO/N_2 fills fully the reactor and the vaporization device was calculated and determined as a duration for CO addition. During the experiments, NO/N_2 was input until the gas flow was constant, at the moment, the CO was pumped into the vaporization device lasting a duration of Δt.

And then the flue gas was switched to bypass in order to control the reaction time of NO oxidation. Subsequently, turn on the main path to output the reacted flue gas for detecting the concentrations of NO and NO_2.

2.3 Investigations of Various Influencing Factors

In order to investigate the influences of ferrous and PAA on NO removal, the experiments with different CO constitutions, such as H_2O_2, H_2O_2/PAA and H_2O_2/PAA/$FeSO_4$, were carried out. Due to the generation of hydroxyl radicals mainly depends on the ferrous concentration, the effects of the ferrous concentrations in CO solution, 3×10^{-3}, 5×10^{-3}, 7×10^{-3} and 9×10^{-3} mol/L, were studied. Additionally, a series of experiments on the CO solution pH, 0.53, 1.02, 2.03, 2.98 and 4.04, were conducted to investigate the effect of pH. Based on the actual temperature conditions of a typical coal-fired power plant, seven temperature points, 60, 70, 80, 90, 100, 110 and 120℃ and four SO_2 contents, 520, 1050, 1560 and 2100 mg/m^3, were selected to evaluate the effects of reaction temperature and SO_2 on NO removal. Based on the data of temperature dependent, the apparent activation energy of NO removal was calculated using the Arrhennius equation.

3 Results and Discussion

3.1 NO oxidation

3 Results and Discussion

3.1 NO oxidation

First of all, the reaction mechanism of NO oxidation by vaporized CO was analyzed. The components in CO are H_2O_2, PAA and ferrous, in which, the former

two are oxidants, the later is catalyst. It has been known that the combination of H_2O_2 and ferrous can generate hydroxyl radicals (HO·) (Eq.1) that is an active oxidant produced from ferrous catalyzing H_2O_2. Also, a similar catalytic action between PAA and ferrous can occur, from which, the oxidation potential of PAA is significantly enhanced in the acidic condition [21], of which the product is still hydroxyl radicals (Eq.2). As for H_2O_2 and PAA, their synergy in the acidic condition has been revealed previously, in which, the acetic acid resulting from the reduction or the decomposition of PAA (Eq.3), can participate in the reaction between H_2O_2 and PAA (Eq.4), leading to an inhibition on H_2O_2 decomposition and maintaining the concentration of PAA. Therefore, all of the three components in CO can improve the performance of vaporized CO oxidizing NO.

According to the above analysis, the main oxidation species in CO are concluded as H_2O_2, PAA and HO·; especially HO·due to the reaction rates between HO·and NO are 5.5×10^{14} $M^{-1}s^{-1}$ or 10^8-10^{12} $M^{-1}s^{-1}$ [22]. Furthermore, from the perspective of electrochemical, the standard electrode potentials of H_2O_2 (1.770 V), HO·(2.800 V) and PAA (1.960 V) are far higher than those of NO_2/NO (1.049 V), NO_3^-/NO (0.957 V), NO_2^-/NO (0.460 V) and NO_3^-/NO_2^- (0.835 V), which also shows the feasibility of NO oxidation by vaporized CO (Eqs.5-8) [23-29]. After oxidation, the just generated oxidation products are rapidly absorbed by $Ca(OH)_2$ with producing $Ca(NO_3)_2$ and $Ca(NO_2)_2$ (Eqs.9-11).

$$Fe^{2+} + H_2O_2 \rightarrow Fe^{3+} + HO^{\bullet} + OH^- \quad (1)$$

$$Fe^{2+} + CH_3COOOH \rightarrow Fe^{3+} + CH_3COO^- + HO^{\bullet} \quad (2)$$

$$M + CH_3COOO^- \rightarrow MO + CH_3COO^- \quad (3)$$

$$H_2O_2 + CH_3COO^- \rightarrow H_2O + CH_3COOO^- \quad (4)$$

$$NO + HO^{\bullet} \rightarrow NO_2 + H^{\bullet} \quad (5)$$

$$NO_2 + HO^{\bullet} \rightarrow NO_3^- + H^+ \quad (6)$$

$$2NO + 3H_2O_2 \rightarrow 2NO_3^- + 2H^+ + 2H_2O \quad (7)$$

$$NO + CH_3COOO^- \rightarrow NO_2 + CH_3COO^- \quad (8)$$

$$Ca(OH)_2 + 2NO_2 \rightarrow Ca(NO_2)_2 + H_2O \quad (9)$$

$$Ca(OH)_2 + 2HNO_2 \rightarrow Ca(NO_2)_2 + 2H_2O \quad (10)$$

$$Ca(OH)_2 + 2HNO_3 \rightarrow Ca(NO_3)_2 + 2H_2O \quad (11)$$

3.2 Reaction Order

The NO removal by vaporized CO as a function of reaction time is shown in Fig. 2. It can be found that the typical NO depletion appears to be exponential to the reaction time, indicating that the depletion conforms to the pseudo-first-order kinetics pattern in a rapid depletion zone (1-2 half-lives) with respect to NO. Obviously, the oxidation rate of NO dominated the NO depletion rate. Therefore, the overall rate of NO depletion can be expressed as followed (Eqs.12-13).

$$-\frac{d[NO]}{dt} = k_{obs}[NO] \quad (12)$$

$$k_{obs} = k_1[\cdot OH] + k_2[H_2O_2] + k_3[PAA] \quad (13)$$

Where k_{obs} is the pseudo-first-order rate constant that represents an overall rate of the NO removal by a variety of oxidizing agents (e.g., H_2O_2, PAA, and HO·) produced in the system; *[H_2O_2]*, *[PAA]* and *[HO·]* are the concentrations of H_2O_2, PAA, and HO·; mmol/m^3; *[NO]* is the concentration of NO at any time, mg/m^3.

The reaction order of NO oxidation could be calculated by using the initial rate method. A series of curves of the NO depletion versus reaction time under various initial NO concentrations were obtained, from which, the initial rates (r_0) were obtained via the reaction 15. And then the reaction order could be calculated by integrating the differential form of the reaction 16. Reaction 17 expresses the relation of $lg(-d_c/d_t)$ and lgc, in which, n is the reaction order with respect to NO. As shown in Fig. 2, the determined reaction order of NO is 1.119, R^2 is 0.998, indicating that the reaction order can be considered as pseudo-first-order kinetics.

$$c = f(t) \quad (14)$$

$$r_0 = \frac{dC_0}{dt} = \frac{df(t)_{t=0}}{dt} \quad (15)$$

$$r_0 = -\frac{dC_0}{dt} = k' c_0^n \quad (16)$$

$$\lg(-\frac{dC_0}{dt}) = \lg k' + n \lg c_0 \quad (17)$$

Where c and c_0 are the NO concentrations at each time and at t=0, respectively, mg/m^3; r_0 is the rate of NO depletion at t=0, $ppm^{-1}\ s^{-1}$; k' is the rate that represents an overall rate of the NO removal by a variety of oxidizing agents (e.g., H_2O_2, PAA, and HO·) produced in the system, $ppm^{1-n}\ s^{-1}$; n is the NO reaction order.

3.3 Effect of the CO constitution

The effect of CO constitution on NO removal was investigated. The experimental conditions are shown in Table. 1. It can be seen from Fig. 3 that, for any particular constitution, the NO depletion exhibits a pseudo-first-order pattern (R^2=0.99). When H_2O_2 is used as the oxidant, the pseudo-first-order rate constant is 0.01093 s^{-1}, which is the minimum among the three tests. When the CO is made up of PAA and H_2O_2, the

rate constant increases to 0.01486 s^{-1}. However, the highest rate constant of 0.02234 s^{-1} is obtained when the CO consists of PAA, H_2O_2 and ferrous. Therefore, the additions of ferrous and PAA can significantly accelerate NO oxidation rate. As for the efficiency, a similar trend is also observed in Fig. 3, the efficiencies are 59.3%, 79.7% and 87.2% with regarding the CO constitutions of H_2O_2, H_2O_2/PAA and H_2O_2/PAA/ferrous. Therefore, the promotion of ferrous and PAA on the rate and the efficiency of NO oxidation was demonstrated, the functional mechanism owing to ferrous and PAA was shown in section 3.1.

It is important to investigate the effect of ferrous concentration on NO removal because the amount of HO · generation is directly affected by the ferrous addition. Therefore, a series of experiments with four ferrous concentrations were conducted at a fixed NO concentration of 550 mg/m^3. It can be seen from Table. 1 and Fig. 4 that the rate constants are 0.01107, 0.02234, 0.02348 and 0.02706 s^{-1} with respect to the ferrous concentrations of 3, 5, 7 and 9 mmol/L, indicating that the oxidation rate is increased evidently as the ferrous concentration rise. Fig. 4 also shows the dependent of removal efficiency on ferrous concentration. It can be found that the removal efficiency increases in the ferrous concentration range of 3 to 5 mmol/L, but declines in the concentration range of 5 to 9 mmol/L. The experimental phenomenon revealed that more ferrous was beneficial for promoting the oxidation rate rather than the removal efficiency, which was due to that more ferrous could generate more hydroxyl radicals in a short time, resulting in an increase of oxidation rate; however, the ferrous-induced side reactions [25] resulting from excessive ferrous, such as the

quenching of hydroxyl radicals (Eq.18) and the decomposition of H_2O_2 (Eq.19), would consume lots of effective oxidants and decrease the oxidizability of CO, which leaded to a decline of NO removal efficiency. Not only to that, the generated OH^- via the reaction 18 may destroy the catalytic function of ferrous because of the ferrous precipitation, meanwhile, the H_2O_2 decomposition also would be further aggravated (Eqs.18, 20-21).

$$Fe^{2+} + HO^{\bullet} \rightarrow HO^- + Fe^{3+} \quad (18)$$

$$FeHO_2^{2+} + H_2O_2 \rightarrow Fe(OH)(HO_2)^+ + H^+ \quad (19)$$

$$H_2O_2 \rightarrow HO_2^- + H^+ \quad (20)$$

$$H_2O_2 + HO_2^- \rightarrow OH^- + O_2 + H_2O \quad (21)$$

3.4 Effect of Reaction Temperature

The effect of reaction temperature on NO removal was investigated. The pseudo-first-order kinetics rate constants under various reaction temperatures were shown in Table. 2. It can be seen from Fig. 5 that as the temperature increases from 333 to 393 K, the rate constant increases from 0.00946 to 0.01980 s^{-1} step by step. Fig. 5 also shows the dependent of removal efficiency on the reaction temperature, it can be found that the lower temperature in the range of 333-363 K has an obvious promotion on the NO removal efficiency, while the higher temperature in the range of 363-393 K plays an inhibition role. Thereby the optimal temperature was 363 K, which was consistent with the actual temperature conditions of ESP outlet, indicating that the vaporized CO had a potential to couple with the ESP system to realize the simultaneous removal of SO_2 and NO. During the experiments, some phenomenon of

244 temperature dependent occurred as the temperature variation, i.e. the elevated
245 temperature in the low temperature range could promote the vaporization rate of CO,
246 the reactants diffusion and the chemical reaction rate; nevertheless, the excessive
247 temperature was unfavorable for the chemical reaction because of the intense
248 decompositions of the reactants and the increase of mass transfer resistance between
249 the oxidation products and $Ca(OH)_2$.

250 As shown in Fig. 6, obviously, lnk_{obs} decreases linearly with *1/T*, therefore,
251 which is fitted to an Arrhenius model (Eq.22). After fitting, the apparent activation
252 energy was 14.1 kJ/mol and the *lnA* was 0.58. Compared with some other apparent
253 activation energies of NO oxidation obtained in previous researches, such as the 42.5
254 kJ/mol for $NaClO_2$ [30], the 27.8 kJ/mol for H_2O_2/NaOH [31], the apparent activation
255 energy of vaporized CO oxidizing NO was lower. And the following reasons may
256 account for the phenomena: compared with the wet bubble reaction system, the
257 proposed novel method had an advantage of larger contact area between the oxidants
258 and NO resulting from the vaporization process. In addition to that, the oxidation
259 potential and reactivity of ·OH are far higher than ClO_2, ClO_2^- and HO_2^- employed by
260 predecessors. Therefore, the reaction barrier of NO oxidation in our reaction system
261 was much lower.

262 $$k = A \times \exp(-\frac{Ea}{RT}) \quad (22)$$

263 Then the log-type was deduced as followed (Eq.23):

264 $$\ln k = \ln A - Ea/RT \quad (23)$$

265 Where *A* is the pre-exponential factor, *Ea* is the apparent activation energy, *R* is

the universal gas constant, and *T* is the absolute temperature.

3.5 Effect of pH

The pH has a significant influence on the oxidation potentials of H_2O_2 and PAA and the stability of ferrous. Therefore, the effect of CO pH on NO removal was investigated, as shown in Fig. 7 and Table. 2. It can be seen that the rate constants are 0.01423, 0.00909, 0.00698, 0.00496 and 0.00343 s^{-1}, responding to the pH of 0.5, 1.0, 2.0, 3.0 and 4.0. Apparently, the lower pH is favorable for increasing the oxidation rate. Similarly, as shown in Fig. 7, the removal efficiency is also sharply decreased from 90.3% to 42.1% as a same variation of pH, which may be due to the following reasons: 1) at a higher solution pH, H_2O_2 was rapidly decomposed as HO_2^- (Eq.20) [32-33], which could adversely accelerate the H_2O_2 decomposition via the reaction 21 [34] and consume ·OH (Eq.24), from which, the oxidizability of the reaction system was decreased with the solution pH increasing. 2) similarly, the elevated pH also had a great inhibition on PAA and ferrous, as discussed in the section 3.1 and the section 3.3.

$$HO^{\bullet} + HO_2^- \rightarrow OH^- + HO_2^{\bullet} \quad (24)$$

3.6 Effect of SO_2 Concentration

SO_2 is a coexistence gas in coal-fired flue gas and has a potential to affect NO removal. Therefore, the experiments with four SO_2 concentrations, 520, 1050, 1560 and 2100 mg/m^3, were conducted to investigate the effect of SO_2 on NO removal. It can be seen from Fig. 8 and Table. 2 that SO_2 has no significant influence on the oxidation rate, but the higher SO_2 concentration in the range of 1050 to 2100 mg/m^3

has a slight inhibition on the NO removal efficiency, which may be a consequence of the competition reaction between SO_2 and NO for the limited oxidants. Generally, the vaporized CO exhibited a good performance on the adaption of SO_2 variation. Hence, the proposed method can be adaptive to the various coal-types and working conditions of boiler.

4 Conclusions

This study made an effort to explore the macrokinetics of NO oxidation by a vaporized H_2O_2-based complex oxidant (CO). The reaction order was 1.119 with respect to NO, which could be considered as the pseudo-first-order kinetics in a rapid depletion zone (1-2 half-lives). The effects of the CO constitution, the ferrous concentration, the reaction temperature, the pH of CO and the SO_2 concentration on NO removal were investigated experimentally. The rate constants of temperature dependent were well fitted to an Arrhenius model, from which, the apparent activation energy of NO oxidation was calculated as 14.1 kJ/mol. The experimental results demonstrated that the novel process can rapidly and effectively remove NO, which provided a viable alternative option to reduce the NO_x emission from coal-fired power plants.

Acknowledgments

The authors appreciate the financial support by a grant from the National High Technology Research and Development Program of China (863 Program, No. 2013AA065403), Hebei provincial Natural Science Foundation, P. R. China (B2011502027), Program for Changjiang Scholars and Innovative Research Team in

University (IRT1127) and Zhejiang Provincial Engineering Research Center of Industrial Boiler & Furnace Flue Gas Pollution Control, Hangzhou, P. R. China (311202).

References

[1] S.J. Chung, K.C. Pillai, I.S. Moon, A sustainable environmentally friendly NO_x removal process using Ag(II)/Ag(I)-mediated electrochemical oxidation, Sep. Purif. Technol. 65 (2009) 156–163.

[2] M. Govindan, S.J. Chung, Il.S. Moon, Simple Technical Approach for Perpetual Use of Electro generated Ag(II) at Semi pilot Scale: Removal of NO and SO_2 as a Model System, Ind. Eng. Chem. Res. 51 (2012) 2697–2703.

[3] P. Davini, SO_2 and NO_x adsorption properties of activated carbons obtained from a pitch containing iron derivatives, Carbon. 39 (2001) 2173–2179.

[4] Q. Tang, Z.G. Zhang, W.P. Zhu, Z.D. Cao, SO_2 and NO selective adsorption properties of coal-based activated carbons, Fuel. 84 (2005) 461–465.

[5] K. Krishna, M. Makkee, Coke formation over zeolite and CeO_2-zeolite and its influence on selective catalytic reduction of NO_x, Appl. Catal. B 62 (2005) 35-44.

[6] M.J. Sang, D.K. Sang, Removal of NO_x and SO_2 by CuO/γ-Al_2O_3 sorbent/catalyst in a fluidized-bed reactor, Ind. Eng. Chem. Res. 39 (2000) 1911–1916.

[7] L. Wang, W.R. Zhao, Z.B. Wu, Simultaneous absorption of NO and SO_2 by FeII EDTA combined with Na_2SO_3 solution, J. Chem. Eng. 132 (2007) 227–232.

[8] X.L. Long, W.D. Xiao, W.K. Yuan, Kinetics of gas–liquid reaction between NO

and $Co(NH_3)_6^{2+}$, J. Hazard. Mater. B 123 (2005) 210–216.

[9] H. Chu, T.W. Chien, B.W. Twu, The absorption kinetics of NO in $NaClO_2$/NaOH solutions, J. Hazard. Mater. B 84 (2001) 241–252.

[10] J.C. Wei, Y.B. Luo, B. Yu, Removal of NO from flue gas by wet scrubbing with $NaClO_2$/$(NH_2)_2CO$ solutions, J. Ind. Eng. Chem. 15 (2009) 16–22.

[11] Y. Zhao, T.X. Guo, Z.Y. Chen, Y.R. Du, Simultaneous removal of SO_2 and NO using M/$NaClO_2$ complex absorbent, Chem. Eng. J. 160 (2010) 42–47.

[12] Y. Zhao, Y.H. Han, T.Z. Ma, T.X. Guo, Simultaneous Desulfurization and Denitrification from Flue Gas by Ferrate (VI), Environ. Sci. Technol. 45 (2011) 4060–4065.

[13] C. Brogren, H.T. Karlsson, I. Bjerle, Absorption of NO in an alkaline solution of $KMnO_4$, Chem. Eng. Technol. 20 (1997) 396–402.

[14] P. Fang, C.P. Cen, Z.X. Tang, P.Y. Zhong, D.S. Chen, Z.H. Chen, Simultaneous removal of SO_2 and NO_x by wet scrubbing using urea solution, Chem. Eng. J. 168 (2011) 52–59.

[15] Y.X. Liu, J. Zhang, C.D. Sheng, Y.C. Zhang, L. Zhao, Simultaneous removal of NO and SO_2 from coal-fired flue gas by UV/H_2O_2 advanced oxidation process, Chem. Eng. J. 162 (2010) 1006–1011.

[16] Y.X. Liu, J. Zhang, Photochemical Oxidation Removal of NO and SO_2 from Simulated Flue Gas of Coal-Fired Power Plants by Wet Scrubbing Using UV/H_2O_2 Advanced Oxidation Process, Ind. Eng. Chem. Res. 50 (2011) 3836–3841.

354 [17] C.D. Cooper, C.A. Clausen, L. Pettey, Investigation of UV enhanced H_2O_2
355 oxidation of NO_x emissions, Environ. Eng. 128 (2002) 68–72.
356 [18] Y.S. Mok, Absorption–reduction technique assisted by ozone injection and
357 sodium sulfide for NO_x removal from exhaust gas, Chem. Eng. J. 118 (2006)
358 63-67.
359 [19] P. Fang, C.P. Cen, X.M Wang, Z.J. Tang, Z.X. Tang, D.S. Chen, Z.H. Chen,
360 Simultaneous removal of SO_2, NO and Hg^0 by wet scrubbing using urea+$KMnO_4$
361 solution, Fuel. Process. Technol. 106 (2013) 645–653.
362 [20] X.H. Xua, Q.F. Ye, T.M. Tang, D.H. Wang, Hg^0 oxidative absorption by $K_2S_2O_8$
363 solution catalyzed by Ag^+ and Cu^{2+}, J. Hazard. Mater. 158 (2008) 410–416.
364 [21] E.S. Huyser, G.W. Hawkins, Ferrous Ion Catalyzed Oxidations of 2-Propanol
365 with Peroxyacetic Acid, J. Org. Chem. 48 (1983) 1705-1708.
366 [22] Y.X. Liu, J. Zhang, C.D. Sheng, Study on the Kinetics of NO Removal from
367 Simulated Flue Gas by a Wet Ultraviolet/H_2O_2 Advanced Oxidation Process,
368 Energy. Fuel. 25 (2011) 1547–1552.
369 [23] E.S. Hwang, J.N. Cash, M.J. Zabik, Ozone and Hydrogen Peroxyacetic Acid
370 Treatment To Reduce or Remove EBDCs and ETU Residues in a Solution, J.
371 Agric. Food Chem. 49 (2001) 5689-5694.
372 [24] E.S. Huyser, G.W. Hawkins, Ferrous ion catalyzed oxidations of 2-propanol with
373 peroxyacetic acid, J. Org. Chem. 48 (1983) 1705-1708.
374 [25] B. Ensing, F. Buda, E.J. Baerends, Fenton-like Chemistry in Water: Oxidation
375 Catalysis by Fe(III) and H_2O_2, J. Phys. Chem. A 107 (2003) 5722-5731.

376 [26] M. Kitis, Disinfection of wastewater with peracetic acid: a review, Environ. Int.
377 30 (2004) 47-55.
378 [27] J.C. Farrand, D. Johnson, Peroxyacetic acid oxidation of 4-methylphenols and
379 their methyl ethers, J. Org. Chem. 36 (1971) 3606-3612.
380 [28] G.B. Payne, P.H. Williams, Notes-reaction of mesityl oxide with peroxyacetic
381 acid, J. Org. Chem. 24 (1959) 284-286.
382 [29] J.D. Laat, T.G. Le, Kinetics and Modeling of the Fe(III)/H_2O_2 System in the
383 Presence of Sulfate in Acidic Aqueous Solutions, Environ. Sci. Technol. 39
384 (2005) 1811-1818.
385 [30] F. Liu, Experimental and Mechanism Study on Simultaneous Removal of SO_2
386 and NO_x using jet bubble reactor. North China Electric Power University, 2009.
387 [31] T.X. Guo, Experimental Investigation on Simultaneous Removal SO_2 and NO_x in
388 Liquid Phase by New-type Complex Absorbent. North China Electric Power
389 University, 2011.
390 [32] Q.H. Hu, C.L. Zhang, Z.R. Wang, Y. Chen, K.H. Mao, X.Q. Zhang, Y.L. Xiong,
391 M.J. Zhu, Photodegradation of methyl tertbutyl ether (MTBE) by UV/ H_2O_2 and
392 UV/TiO_2. J. Hazard. Mater. 154 (2008) 795–803.
393 [33] F. Yuan, C. Hu, X.X. Hu, ; J.H. Qu, M. Yang, Degradation of selected
394 pharmaceuticals in aqueous solution with UV and UV/H_2O_2. Water. Res. 43
395 (2009) 1766–1774.
396 [34] W.M. Wang, J.Song, X. Han, Schwertmannite as a new Fenton-like catalyst in the
397 oxidation of phenol by H_2O_2. J. Hazard. Mater. 262 (2013) 412–419.

Figures

Fig. 1

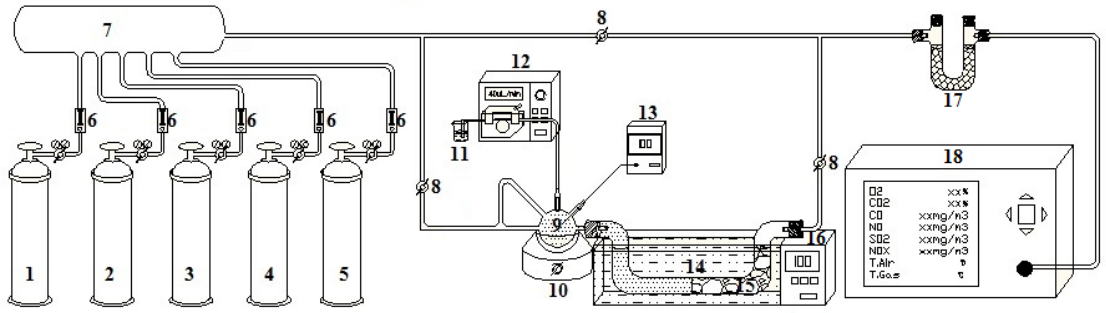

Schematic diagram of the experimental apparatus of the fix-bed.

1-5 CO_2, N_2, SO_2, NO, O_2 gas cylinders; 6-flowmeters; 7-buffer bottle; 8-tee joint; 9-vaporization device; 10-thermal control electric heater; 11-CO solution; 12-peristaltic pump; 13-thermal couple; 14-reactor; 15-$Ca(OH)_2$; 16-thermostat oil bath; 17-dryer; 18-flue gas analyzer.

Fig. 2

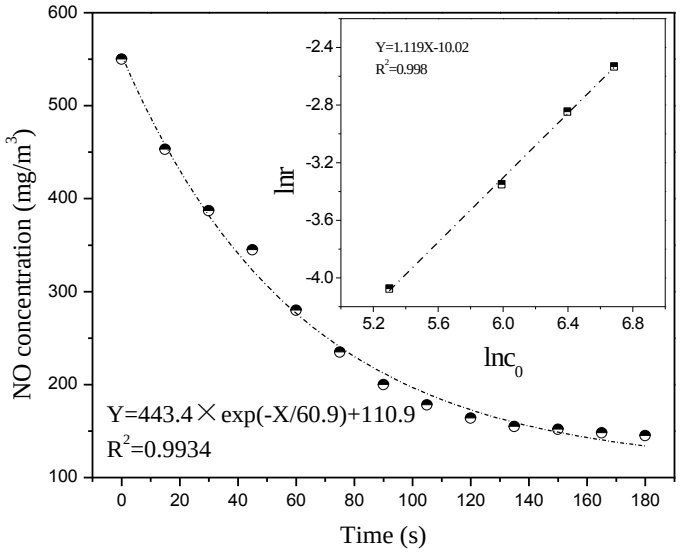

Determination of reaction order with respect to NO.

Simulated flue gas inlet velocity is 4.0 L/min, adding rate of CO is 200μl/min; CO solution pH is 0.7, reaction temperature is 363 K, NO concentration is 550 mg/m^3.

Fig. 3

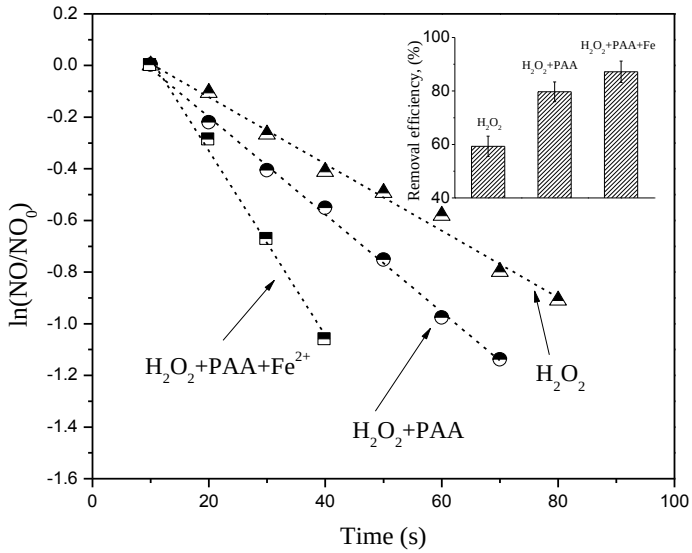

Pseudo-first-order depletion of NO at various CO constitutions.

Simulated flue gas inlet velocity is 4.0 L/min, adding rate of CO is 200μl/min; CO solution pH is 0.7, reaction temperature is 363 K, NO concentration is 550 mg/m^3.

425 **Fig. 4**

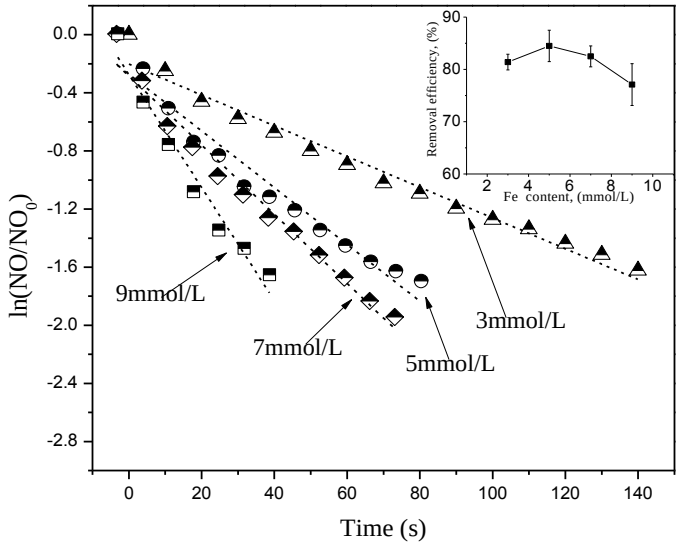

426

427 Pseudo-first-order depletion of NO at various ferrous concentrations.

428 Simulated flue gas inlet velocity is 4.0 L/min, adding rate of CO is 200μl/min; CO

429 solution pH is 0.7, reaction temperature is 363 K, NO concentration is 550 mg/m^3.

430

431 **Fig. 5**

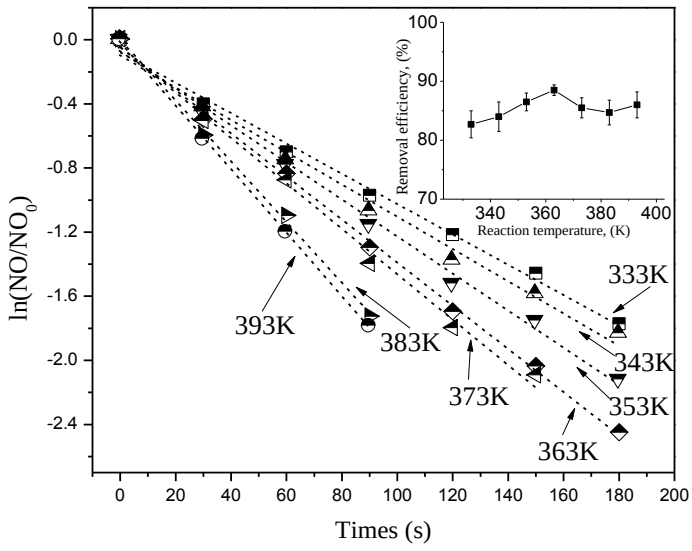

432

433 Pseudo-first-order depletion of NO under various reaction temperatures.

434 Simulated flue gas inlet velocity is 4.0 L/min, adding rate of CO is 200μl/min; CO

435 solution pH is 0.7, NO concentration is 550 mg/m^3.

436

437 **Fig. 6**

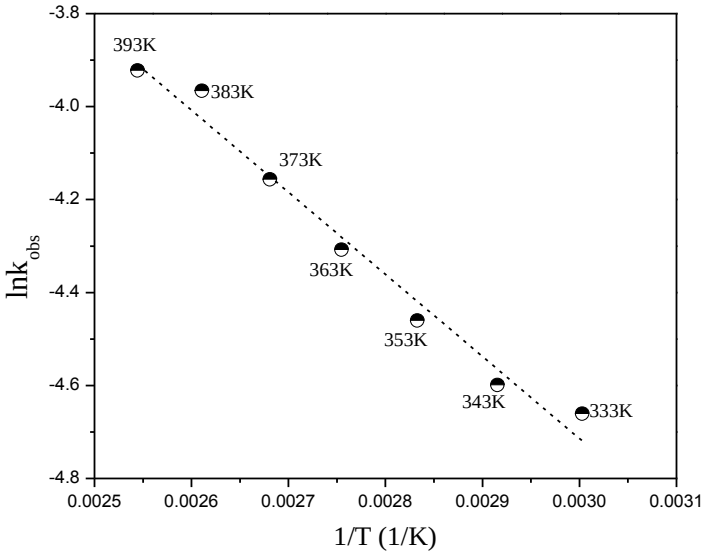

438

439 Arrhenius plots for the removal of NO.

440 Simulated flue gas inlet velocity is 4.0 L/min, adding rate of CO is 200 μl/min; CO

441 solution pH is 0.7, NO concentration is 550 mg/m^3.

442

443

444

445

446

447

448 **Fig. 7**

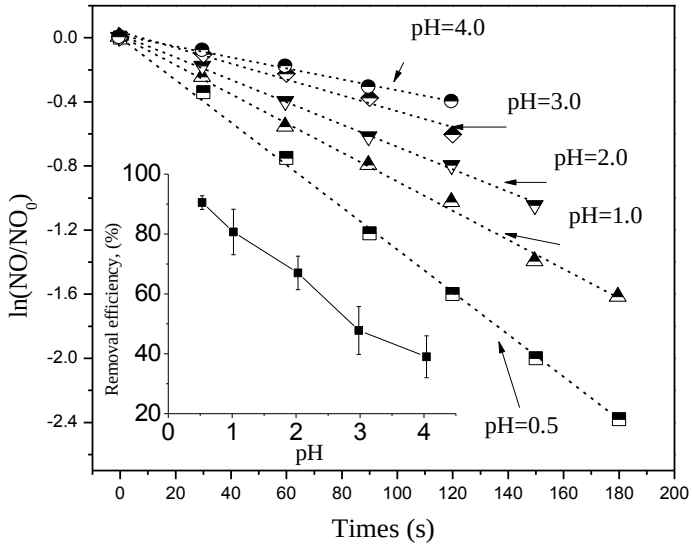

449

450 Pseudo-first-order depletion of NO under various pH.

451 Simulated flue gas inlet velocity is 4.0 L/min, adding rate of CO is 200 μl/min;

452 reaction temperature is 363 K, NO concentration is 550 mg/m^3.

453

454 **Fig. 8**

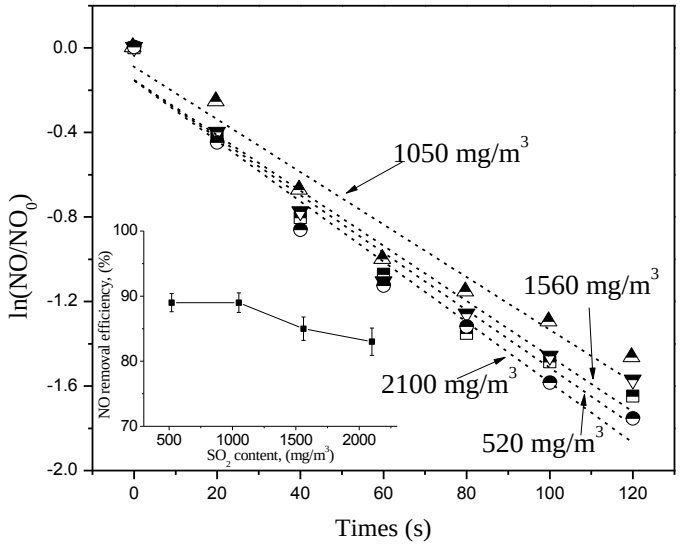

455

Pseudo-first-order depletion of NO under various SO_2 contents.

Simulated flue gas inlet velocity is 4.0 L/min, adding rate of CO is 200 μl/min; reaction temperature is 363 K, NO concentration is 550 mg/m^3.

Tables

Table 1

Pseudo-first-order kinetics parameters of NO removal at various CO constitutions.

Test	CO constitution			$t_{1/2}$, s	Rate constant (k,s^{-1})	Denitrification efficiency	Correlation coefficient, R^2
	H_2O_2, mol/L	PAA, mol/L	Fe^{2+}, mmol/L				
1	4	0	0	63.4	0.01093	59.3%	0.98993
2	4	1	0	46.6	0.01486	79.7%	0.99725
3	4	1	5	31	0.02234	87.2%	0.99301
4	4	1	3	62.6	0.01107	81.4%	0.98083
5	4	1	7	51.4	0.02348	82.5%	0.98227
6	4	1	9	25.6	0.02706	77.1%	0.95897

Table 2

Pseudo-first-order kinetics parameters of NO removal under various reaction conditions

	Reaction conditions			$t_{1/2}$, s	Rate constant (k, s^{-1})	Removal efficiency	Correlation coefficient, R^2
	Temperature (K)	pH	NO/ SO_2 (mg/m^3)				
1	333	0.7	550	73.3	0.00946	83.2	0.99264
2	343	0.7	550	68.9	0.01006	84.3	0.98695
3	353	0.7	550	60	0.01156	86.7	0.99432
4	363	0.7	550	51.5	0.01346	88.9	0.99765
5	373	0.7	550	45.7	0.01517	85.3	0.99266
6	383	0.7	550	36.6	0.01895	84.9	0.99738
7	393	0.7	550	35	0.01980	85.4	0.99967
8	363	0.5	550	48.7	0.01423	90.3	0.98734
9	363	1.0	550	76.2	0.00909	81.1	0.99673
10	363	2.0	550	99	0.00698	68.7	0.99785
11	363	3.0	550	140	0.00496	48.7	0.96773
12	363	4.0	550	202	0.00343	42.1	0.99213
13	363	0.7	550/520	45.9	0.01511	88.6	0.95714
14	363	0.7	550/1050	51.6	0.01344	88.3	0.95388
15	363	0.7	550/1560	53	0.01308	84.7	0.94676
16	363	0.7	550/2100	48.5	0.01429	85.5	0.96450

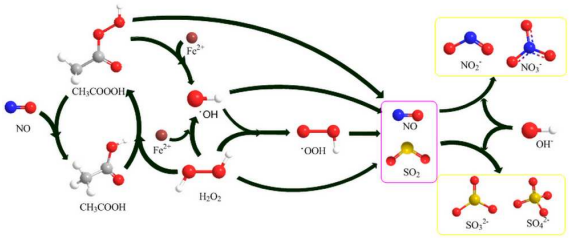

Macrokinetics and feasibility of denitrification using a vaporized enhanced-Fenton reagent were determined.